Scale adaptive simulation of unsteady cavitation flow around a plane convex hydrofoil with a semi-cylindrical obstacle

Scale adaptive simulation of unsteady cavitation flow around a plane convex hydrofoil with a semi-cylindrical obstacle

V Hidalgo[1,3,4], X Escaler[2], A Díaz[3], X Luo[4], S Simbaña[3], D Márquez[3], P Hernandez[5] and E Valencia[1]

[1] Departamento de Ingeniería Mecánica, Escuela Politécnica Nacional, Quito 170525, Ecuador

[2] Centre for Industrial Diagnostics and Fluid Dynamics, UPC, Barcelona, Spain

[3] Laboratorio Informática–Mecánica, Escuela Politécnica Nacional, Quito 170525, Ecuador

[4] State Key Laboratory of Hydro Science & Engineering, Tsinghua University, Beijing, China

[5] Carrera de Ingeniería Automotriz, Facultad de Ingeniería y Ciencias Aplicadas, Universidad Técnica Norte, Ibarra 100105, Ecuador

Correspondence: victor.hidalgo@epn.edu.ec; Tel.: +593-982-491-193

Abstract. The present study focuses on the numerical simulation of unsteady cavitating flow around a plane-convex hydrofoil with a semi-cylindrical obstacle, which is based on the cavitation-erosion experiment perform at LMH-EPFL using the vortex cavitation generator tunnel. The turbulence model k-ω SST SAS method, which presents advantages in terms of computational consumption and reproduction of the phenomenon, has been applied in OpenFOAM version 4 to reproduce the unsteady behavior of cavitating flow. Additionally, the Zwart-Gerber-Belamri (ZGB) cavitation model has been applied, based on a previous work where this model was implemented in OpenFOAM. The model is based on Rayleigh Plesset equation, which considers small cavities with changes of void fraction for condensation and vaporization and using empirical calibration numbers based on previous research. Regarding the mesh development, the present work explores two configurations of grid mesh containing hexahedra (hex) and split-hexahedra (split-hex) automatically generated from triangulated surface geometries based on previous numerical studies. The aforementioned method aims to optimize computational demand and phenomenon reproducibility. Results show that the unsteady cavitating flows behavior has been reproduced with good accuracy and shows special details which are important for erosion studies in futures works.

1. Introduction

Hydroelectric power plants are an ecologically and economically method to solve problems related to energy security and energy deficit [1][2]. Moreover, apart from generating electricity, hydroelectric dams regulate water flows, provide fresh water, mitigate the effects of floods and irrigate crops [3]. The kinetic energy of the moving water when it is directed through the turbine, it becomes into mechanical energy. Then, the mechanical energy is converted into electricity in the generator. During the last century, hydropower has become widely use and of great impact on electricity generation for developed countries such as Canada, Switzerland, Sweden, Norway and also for developing countries such as Ecuador and Colombia [4].

The growth of the output power of the Francis turbine is based on the reduction of dimensions to reduce the cost of its components. Therefore, speeds are increased, and cavitation phenomenon are more likely to occur [5]. One of the most important types of cavitation in the field of hydraulic engineering is represented by the so-called hydrodynamic cavitation, where the pressure drop is caused by the local increase in flow velocity [6]. Cavitation can lead to erosion, both phenomena resulting in an increase in the cost of maintenance and undesirably affecting the operation and useful life of hydraulic machines [7] [8]. The phenomenon is a design consideration for a wide variety of devices that handle liquids [9].

Research on unsteady cavitation is of great economic importance in the field of hydraulic machinery since understanding the phenomenon helps to improve machine and equipment designs [10]. Escaler et al. presents for the first time the procedure of erosion test by cavitation in the high-speed tunnel of the laboratory of Hydraulic Machines (LMH-EPFL) of the Federal Polytechnic School of Lausanne (EPFL). The experimental configuration is based on obstacles mounted on the surface of a leading edge of the plane convex hydrofoil, which can accelerate the rate of erosion damage by

cavitation on the flat surface [11]. The unsteady dynamics of cloud cavitation flow around a hydrofoil is investigated using experimental and numerical methods [12]. The numerical method predicts that the impact energy is small if the variation of the cavitation flow is small and that the position of the maximum impact energy moves down with the decrease of the cavitation number until the maximum length of the cavity of the blade becomes longer than the length of the chord [13]. The cloud cavitation area is divided into two parts: a vapor sheet attached at the front of the cavity and an unsteady biphasic mixture in the posterior region during the process of cavity collapse. The increase in local pressure induced by the reentrant jet is the main reason for driving the cloud cavity. The adverse pressure gradient in the posterior area of the cavity is primarily responsible for the generation of the re-entrant jet [12]. These studies showed the structure of unsteady flow and the evolution of cloud cavitation patterns. It was concluded that the cavitation detachment and the violent collapse of the cavity, when the structures enter the region of highest pressure near the vicinity of the solid surface is the area most affected by vibrations and erosion. In this context, computational fluid dynamics (CFD) is shown as a fundamental tool in the study of cavitation, due to the costs and limitations of the experiments [14].

A small group of tools for numerical simulation take advantage of free and open source software (FOSS). There is open source software such as OpenFOAM, which gives users the freedom to modify and improve the program. Hidalgo V. et al. implemented and validated the ZGB cavitation model as an OpenFOAM library using the implicit large eddy simulation (ILES) turbulence model [15]. Accurate simulations of the partial cavitation detachment process were obtained, which is the main mechanism of erosion. In addition, the author proposed the cavitation-erosion model based on the assumption of homogeneous flow [16]. The obtained results present good accuracy with observed experimental results.

Based on the above, this work performs the numerical study of the cavitation flow around a plane convex hydrofoil with semi-cylindrical obstacle using the SAS turbulence model implemented by Hidalgo V [17]. The results are compared graphically with studies conducted by Hidalgo V. [16] and Escaler X. [11].

2. Model description

2.1. Reynolds-Averaged Navier-Stokes Equations

The constitutive equations used in the Reynolds-averaged Navier–Stokes (RANS) equations are referred to as turbulence models [18]. The model consists of the filtered momentum equation (1) and filtered continuity equation (2).

$$\frac{\partial \overline{u_i}}{\partial t} + \overline{u_j}\frac{\partial \overline{u_i}}{\partial x_j} = -\frac{\partial \overline{p}}{\partial x_i} + \nu\frac{\partial^2 \overline{u_i}}{\partial x_j \partial x_i} - \frac{\partial \tau_{ij}}{\partial x_j}, \tag{1}$$

$$\frac{\partial \overline{u_i}}{\partial x_i} = 0\,, \tag{2}$$

where u_i is the fluid velocity, p is the pressure divided by the density, ν is the fluid kinematic viscosity, and τ_{ij} is the Reynolds-stress tensor term divided by the density that incorporates the effects of turbulent motions on the mean stresses [19].

2.2. Scale Adaptative Simulation

The Scale-Adaptive Simulation (SAS) concept is based on the introduction of the von Karman length-scale into the turbulence scale equation [20], it can be expressed as

$$L_{\nu K} = \kappa \left| \frac{\overline{U}'}{\overline{U}''} \right|, \tag{3}$$

where κ is the von Kármán constant and it is usually equal to 0.41 according to Xu et al. [21] and Hidalgo et al. [17] . Menter and Egorov showed that the $\left|\overline{u}''\right|$term is the result of the exact length-scale equation of Rotta. It has also been shown that this term allows the model to operate in a scale-adaptive simulation mode. L_{vK} is a three-dimensional generalization of the boundary layer definition considering a von Kármán length-scale [17], with

$$\overline{u}' = \sqrt{2\overline{S}_{ij}\overline{S}_{ij}}\,, \tag{4}$$

and

$$\overline{u}'' = \sqrt{\frac{\partial^2\overline{u}_k}{\partial x_i^2}\frac{\partial^2\overline{u}_k}{\partial x_j^2}}\,, \tag{5}$$

More details of SAS description are given in [21].

2.3. Zwart-Gerber-Belamri Cavitation Model

The Zwart-Gerber-Belamri model indicated in equation (6) has been written in C++ language and implemented in OpenFOAM [15].

$$\dot{m} = \begin{cases} \dot{m}^+ = F_v \dfrac{3\, r_{nuc}\ (1-\alpha)\rho_v}{R_B}\sqrt{\dfrac{2}{3}\left(\dfrac{p_v - p}{\rho_l}\right)}, & si\ \ p < p_v \\ \dot{m}^- = -F_C \dfrac{3\ \alpha\ \rho_v}{R_B}\sqrt{\dfrac{2}{3}\left(\dfrac{p_v - p}{\rho_l}\right)}, & si\ \ p > p_v \end{cases} \tag{6}$$

Where p and p_v are the pressure and vapor saturation pressure respectively, $F_v = 50$ and $F_c = 0.03$ are the selected calibration constants for vaporization and condensation, $r_{nuc} = 5.0\ x\ 10^{-6}$ is the nucleation site volume fraction, $R_B = 1.0\ x\ 10^{-6}$ m is the typical bubble size in water [23].

3. Methodology

3.1. Geometric model and computational domain

The plane convex hydrofoil (HFC) has 91,1 mm chord length, the profile cross-section has a suction plane and a circular pressure side of radius 110,2 mm [11]. The semicircular obstacle is mounted on the plane surface on the front border profile as shown in Figure 1.

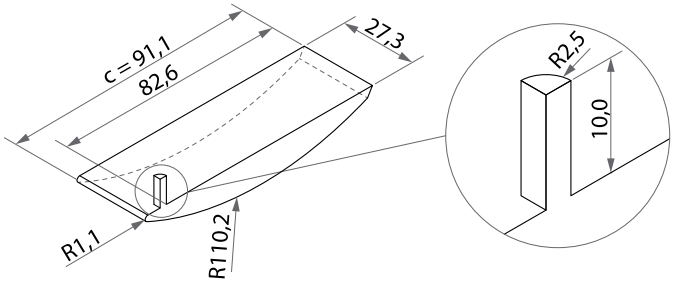

Figure 1. Geometric model dimensions [mm].

The domain is defined in function of the chord length "c" of the hydrofoil. Face names are assigned as "in" and "out" for the flow entrance and exit, "top" and "bottom" for the superior and inferior faces, "wing" for the hydrofoil walls, lastly, "front" and "back" for the symmetry faces, as shown in Figure 2.

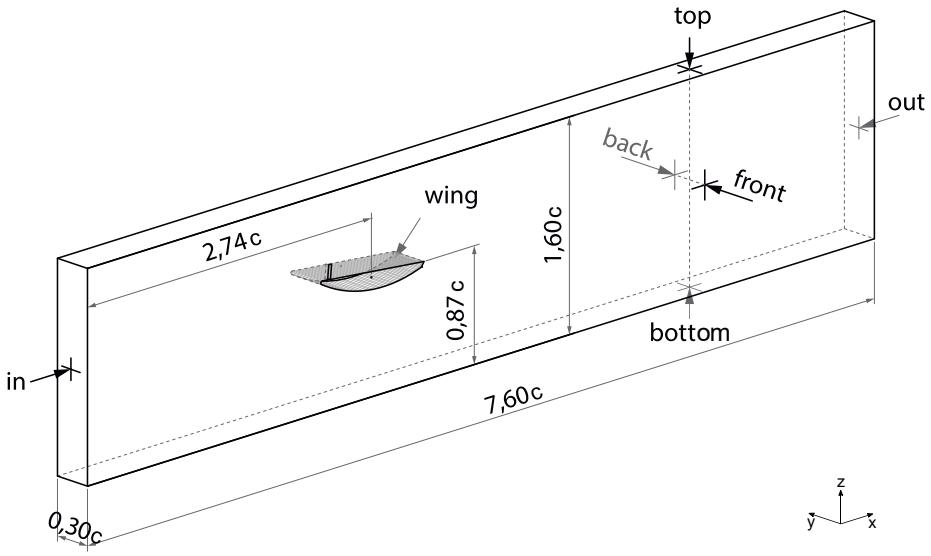

Figure 2. Description of the computational domain HFC [m].

3.2. Mesh Generation

For the study of the unsteady cavitating flow, two hybrid meshes H-type with different combinations of method of the use of the tools SnappyHexMesh and blockMesh. The first configuration is shown in figure 3a, it combines a base mesh generated with blockMesh and it is rotated 3° with respect to the "x" axis. The base mesh is bigger than the computational domain and contains it completely. On the other hand, the tool SnappyHexMesh generates tridimensional meshes using triangular meshes. The geometries are in .stl file format, in this case in, out, bottom, top, front back and wing are divided in two parts. The surfaces of the semi-cylindrical obstacle are named as obs1 and w1 for the hydrofoil surface. The second configuration shown in Figure 3b uses two triangulated geometries obs1 and w1, the other parts of the domain were generated using blockMesh as part of the base mesh and were not rotated. For this case, SnappyHexMesh was used only to refine the surroundings of the triangulated geometries. The rest of the domain remained with uniform cells of the base mesh. Both meshes have 4 levels of refinement and boundary layers around the geometries obs1 and w1.

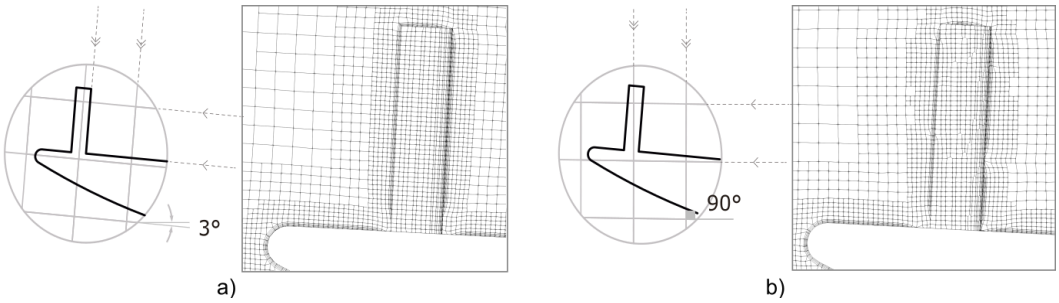

Figure 3. Mesh description, a) mesh 1 (2'443.192 elements) and b) mesh 2 (1'926.841 elements).

The mesh independence study was based on previous studies carried out by Hidalgo et al. [10][14][15].

3.3. Boundary Conditions

Table 1 resumes the conditions used for the cavitation-erosion experiments performed in the Hydraulics Machines laboratory at EPFL. The free flow velocity is represented by U_∞ , the pressure p_∞, the

cavitation number σ, and the angle of attack $\widehat{AOA}$. The chord length of the hydrofoil is defined as "c" [11].

Table 1. Experimental data obtained for the HFC.

Variable	U_∞	p_∞	σ	$\widehat{AOA}$	c
Units	[m/s]	[kPa]		°	[mm]
HFC	35.00	613.60	1.00	3.00	91.10

Table 2 details the boundary conditions of the computational domain used for both meshes. The boundary condition for top and bottom is "slip" whereas for obs1 and w1 "noSlip". This was based on the "Numerical simulation of cavitation erosion on a NACA0015 hydrofoil based on bubble collapse strength" performed by Hidalgo et al [24].

Table 2. Boundary conditions for the computational domain of the HFC.

in	out	front	back	top	bottom	obs1	w1
patch	patch						
Velocity [m/s]	Pressure [kPa]	symmetry	symmetry	wall	wall	wall	wall
U_∞ = 35.0	p_∞= 613.3						

3.4. OpenFOAM Simulation

OpenFOAM 4.1 version was used on the operative system Ubuntu16.04 LTS of Linux based on Debian. The hardware used was a Work Station with Xeon (R) Silver4116 processor with 12 cores and 24 threads, its RAM memory of 128 GB DDR42666 MHz and its interchange memory of 128GB of SSD disk. The scheme shown in Figure 4 is divided in two parts. The first corresponds to the use of OpenFOAM and the vInterPhaseChangeFoam solver for the study of unsteady cavitating flow. The second part is related to results processing with a direct analysis using Paraview o partial analysis using Gnuplot.

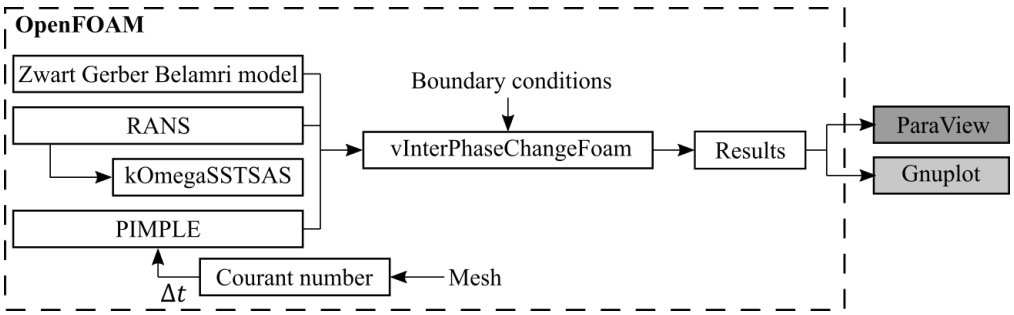

Figure 4. Development of the program on OpenFOAM for the cavitation study

4. Results and discussion

The following results correspond to two study cases. Directories were named as A and B where "mesh1" and "mesh2" are found respectively. The average time for each simulation was 12 hours using 12 processors in parallel.

4.1. Mesh quality

Parameters used to evaluate the mesh quality were the y^+criterion and the hexahedral distortion analysis. The y^+values obtained for "mesh1" were an average of 2.83, a minimum of 0.82; whereas for "mesh2" the values were an average of 2.58 and a minimum of 1.80 which are similar to the ones obtained by Hidalgo et al. [10][14][16]. The hexahedral distortion was analyzed using ParaView and its Mesh Quality filter. Figure 5 shows the distortion results for each mesh. In both cases, the acceptable values are between 0.5 and 1, and the normal range is between 0 and 1 [25].

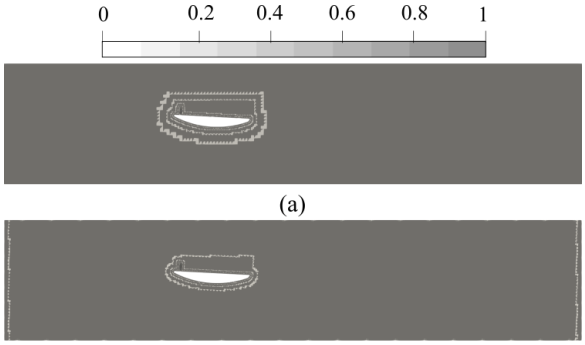

Figure 5. Hexahedral distortion analysis, a) results "mesh 1" and b) results "mesh 2".

4.2. Graphical comparison with previous studies

Validation in both cases was performed based on the comparison of images obtained experimentally and numerically in the studies presented by Hidalgo V [16] and Escaler X [11]. Using the images obtained during postprocessing, a cavity separated in a shape of two elongated arms is identified as shown in Figure 6a. The cavity causes damage on the material surfaces, leaving its characteristic mark described as "rabbit ears", see Figure 6b. The described image is taken as reference start point for the comparison of an unsteady cavitation cycle.

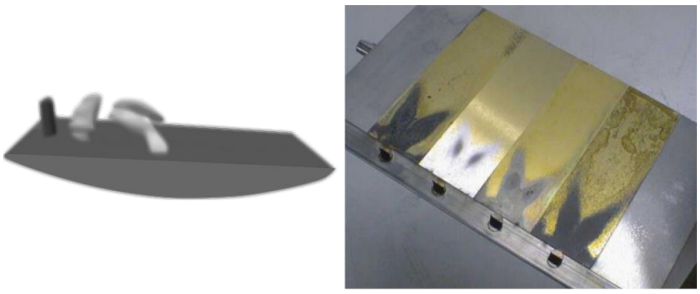

Figure 6. Images used to identify the study start point, a) cavity separated in shape of two elongated arms b) top view of the hydrofoil with obstacles and eroded samples at the end of the experiment.

Once the start point "i" is located, using the plot $V_{cav}/V_{cav,\,max}$ shown in Figure 7 and the postprocessing images, a complete unsteady cavitation cycle is analyzed. Points "i", "ii", "iii", "iv" and "v" are the 5 characteristic moments that depict the development of the separated cavity, whereas "vi", "vii", "viii", "ix" and "x" describe the development of the adjoint cavity.

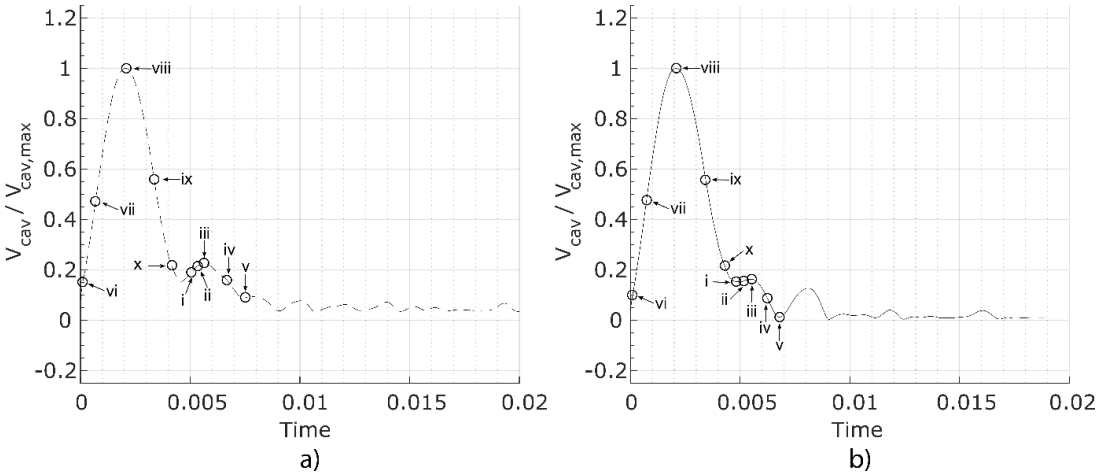

Figure 7. Vapour fraction plot, a) Case A plot b) Case B plot.

Figure 8 shows the images corresponding to the point shown on the plot $V_{cav}/V_{cav,\ max}$. In this case the development, growth and placement of the separated cavity are illustrated. Furthermore, the maximum cavity cycle, the decrease of vapor volume and the lowest point where the vapor volume collapsed are shown. The vapor cavity with elongated arms shape is the shortest along the HFC surface for both cases. This is due to the change of the turbulence model. The ILES model generates more turbulence so that the cavities during the five moments do not resemble to the previous studies. However, they follow the cycle behavior.

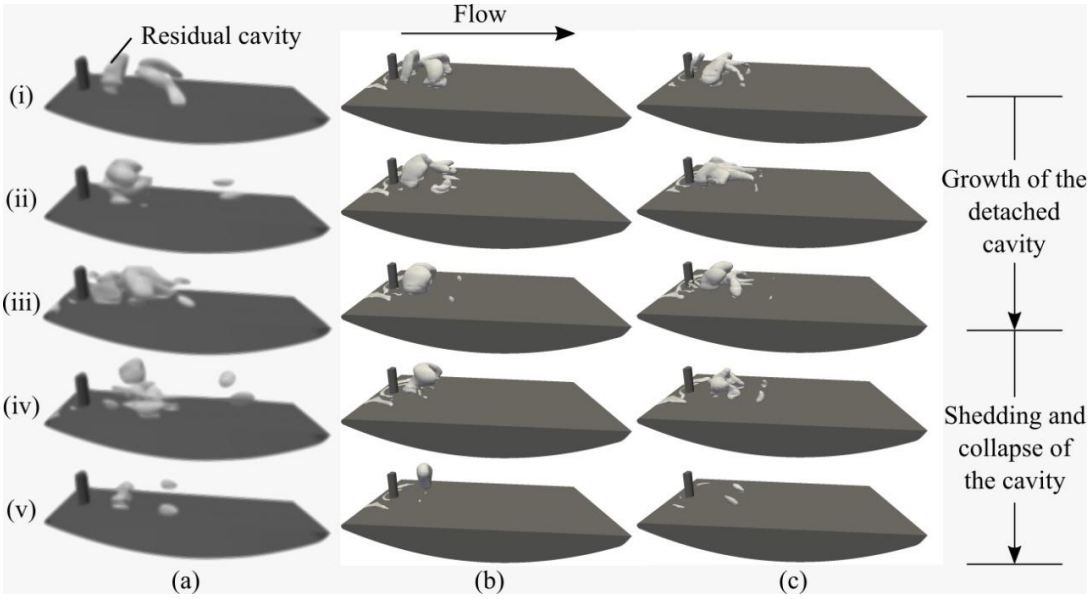

Figure 8. Comparison of the separated cavity evolutive cycle, a) previous studies images, b) case "A" results and c) Case "B" results.

Figure 9 shows the comparison of the vorticity results during growth, detachment and cavity collapse for the three cases. Paraview was used with a Q criterion value of 1 e^{-7} s^{-2}. The image shows the five identified points for the separated cavity analysis. It is observed that the previous studies images have a higher vorticy level, the clouds completely cover the flat surface of the HFC and the semicircular obstacle. Similarly, in the cases "A" and "B" the clouds of vorticity completely cover the obstacle and

show large exposed areas on the flat surface at the back of the HFC. The detachment is low and almost null in “A” and “B”.

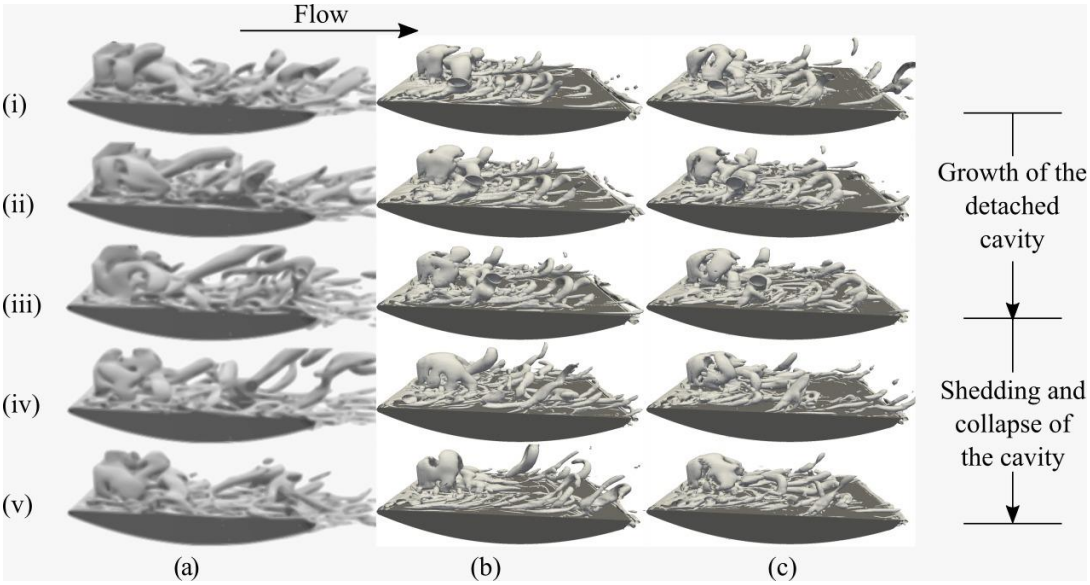

Figure 9. Vorticity according to the Q criterion of the separated cavity, a) images from previous studies, b) results of case A and c) results of case B.

The analysis of the adjoint cavity was performed using the plot $V_{cav}/V_{cav,\,max}$ similar to the one presented for the separated cavity. There are no images from previous studies for the comparison of the adjoint cavity. Figure 10 compares the results of the vapor cavity and vorticy according to the Q criterion for the cases A and B.

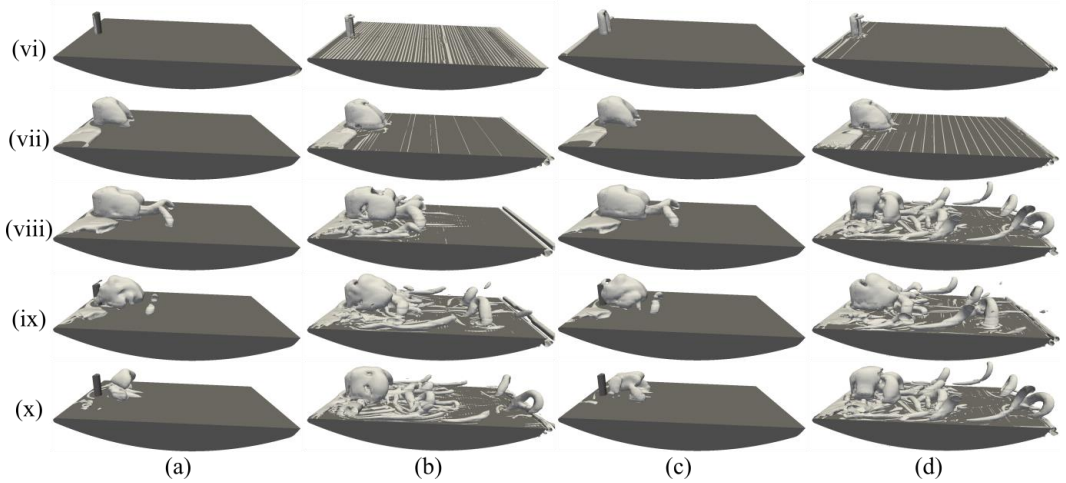

Figure 10. Results of the adjoint cavitation cycle a) case A vapor cavities, b) case A vorticity, c) vapor cavities case B and d) vorticity case B.

In cases A and B, the images of the vapor cavities are similar to the points “vii”, “viii” and “ix”. However, the images in the points “i” and “x” does not coincide by the small deviation in the data

obtained. The vortex evolution at point "ix" is the only one that resembles both cases. The rest of the images present lightly similar characteristics.

5. Conclusions

It was determined that the SAS turbulence model, in comparison of studies which use the ILES model, reproduce the cavitation phenomenon with less vorticity. In this context, it is possible to identify the separated cavity which has a shape of two arms in both cases of the HFC study, the cavities are smaller to the ones found in previous studies due to the use of a different turbulence model. Moreover, it was found that the meshing disposition influences the results when simulating the HFC cases. Better results were obtained when placing the mesh lines parallel and perpendicular to the semicircular surface obstacle.

Finally, the results show that both hybrid meshes used in the HFC cases were able to reproduce in a similar way the evolution of the adjoint cavity and it can be used for future studies on hydraulic machinery.

Acknowledgments: The authors gratefully acknowledge the financial support provided by Escuela Politécnica Nacional for the development of this study, which is part of the research project PIJ 17-13 and project PII-DIM-2019-06.

References

[1] O. Brylina, K. Semenova, and S. Nechitailo, "On issue of hydroelectric power plants," 2018.
[2] S. Algburi, "Energy Science & Technology Vol. 1: Opportunities and ChallengesChapter: 17-Hydropower.Publisher: Studium Press LLC, USA. Editors: J.N. Govil," 2016.
[3] B. Sovacool and W. Götz, "Internationalizing the political economy of hydroelectricity : security , development and sustainability in hydropower states," *Rev. Int. Polit. Econ.*, 2018.
[4] Balat, M. (2006). Hydropower systems and hydropower potential in the European Union countries.
[5] Energy Sources, Part A: Recovery, Utilization and Environmental Effects, 28(10), 965–978. https://doi.org/10.1080/00908310600718833 [5] X. Escaler, E. Egusquiza, M. Farhat, F. Avellan, and M. Coussirat, "Detection of cavitation in hydraulic turbines," *Mech. Syst. Signal Process.*, vol. 20, no. 4, pp. 983–1007, 2006.
[6] C. E. Brennen, *Cavitation and Bubble Dynamics*. 1995.
[7] J. Kozak, P. Rudolf, M. Hudec, D. Stefan, and M. Forman, "Numerical and experimental investigation of the cavitating flow within Venturi tube," *J. Fluids Eng.*, vol. 141, no. April, 2018.
[8] A. Boorsma and S. Whitworth, "Understanding Details of Cavitation," no. June, 2011.
[9] R. Arndt, "Cavitation in fluid machinery and hydraulic structures," pp. 273–328, 1981.
[10] V. Hidalgo, X. Escaler, R. Soto, E. Valencia, E. Cando, and X. W. Luo, "Large eddy simulation of partial cavitation around a 2D plane-convex hydrofoil," *J. Hydrodyn.*, vol. 35, 2015.
[11] X. Escaler, M. Farhat, F. Avellan, and E. Egusquiza, "Cavitation erosion tests on a 2D hydrofoil using surface-mounted obstacles," *Wear*, vol. 254, no. 5–6, pp. 441–449, 2003.
[12] G. Wang and B. Zhang, "Unsteady Dynamics of Cloud Cavitating Flows around a Hydrofoil," no. 9, pp. 1–8, 2009.
[13] N. Ochiai, Y. Iga, M. Nohmi, and T. Ikohagi, "Numerical prediction of cavitation erosion in cavitating flow," *J. Fluids Eng. Trans. ASME*, vol. 135, no. 1, pp. 1–9, 2013.
[14] V. Hidalgo, X. W. Luo, X. Escaler, A. Yu, and E. Valencia, "Study of partial cavitation on a plane-convex hydrofoil with mesh development by using GMSH free software," *ASME/JSME/KSME 2015 Jt. Fluids Eng. Conf. AJKFluids 2015*, vol. 2A, no. December, 2015.
[15] V. Hidalgo, X. W. Luo, X. Escaler, B. Ji, and A. Aguinaga, "Implicit large eddy simulation of unsteady cloud cavitation around a plane-convex hydrofoil," *J. Hydrodyn.*, vol. 27, no. 6, pp. 815–823, 2015.
[16] V. Hidalgo, X. Escaler, E. Valencia, X. Peng, J. Erazo, D. Puga, X. Luo. "Numerical study on unsteady cavitating flow and erosion based on homogeneous mixture assumption," no. May, 2016.
[17] V. Hidalgo *et al.*, "Scale-Adaptive Simulation of Unsteady Cavitation Around a Naca66 Hydrofoil," *Appl. Sci.*, vol. 9, no. 18, p. 3696, 2019.

[18] T. Kajishima and K. Taira, *Reynolds-Averaged Navier–Stokes Equations. Computational Fluid Dynamics, 237–268. doi:10.1007/978-3-319-45304-0_7*. 2016.
[19] G. Alfonsi, "Reynolds-averaged Navier-Stokes equations for turbulence modeling," *Appl. Mech. Rev.*, vol. 62, no. 4, pp. 1–20, 2009.
[20] F. R. Menter and Y. Egorov, "A scale-adaptive simulation model using two-equation models," *43rd AIAA Aerosp. Sci. Meet. Exhib. - Meet. Pap.*, no. January, pp. 271–283, 2005.
[21] C. Y. Xu, T. Zhang, Y. Y. Yu, and J. H. Sun, "Effect of von Karman length scale in scale adaptive simulation approach on the prediction of supersonic turbulent flow," *Aerosp. Sci. Technol.*, vol. 86, pp. 630–639, 2019.
[22] F. R. Menter and Y. Egorov, "The scale-adaptive simulation method for unsteady turbulent flow predictions. part 1: Theory and model description," *Flow, Turbul. Combust.*, vol. 85, no. 1, pp. 113–138, 2010.
[23] V. H. Hidalgo, X. W. Luo, X. Escaler, J. Ji, and A. Aguinaga, "Numerical investigation of unsteady cavitation around a NACA 66 hydrofoil using OpenFOAM," *IOP Conf. Ser. Earth Environ. Sci.*, vol. 22, 2014.
[24] V. Hidalgo, X. Luo, X. Escaler, R. Huang, and E. Valencia, "Numerical simulation of cavitation erosion on a NACA0015 hydrofoil based on bubble collapse strength," *J. Phys. Conf. Ser.*, vol. 656, no. 1, 2015.
[25] C. J. Stimpson, C. D. Ernst, P. Knupp, P. P. Pébay, and D. Thompson, "The Verdict Geometric Quality Library," no. March, 2007.